Role of trap recharge time on the statistics of captured particles

Gregory Handy, Sean D. Lawley, and Alla Borisyuk

Phys. Rev. E **99**, 022420 — Published 25 February 2019

DOI: 10.1103/PhysRevE.99.022420

Role of trap recharge time on the statistics of captured particles

Gregory Handy, Sean D. Lawley, and Alla Borisyuk*
Department of Mathematics, University of Utah, Salt Lake City, UT
(Dated: January 22, 2019)

We consider n particles diffusing freely in a domain. The boundary contains absorbing escape regions, where the particles can escape, and traps, where the particles can be captured. Modeled after biological examples such receptors in the synaptic cleft and ambush predators waiting for prey, these traps, or capture regions, must recharge between captures. We are interested in characterizing the time courses of the number of particles remaining in the domain, the number of cumulative captures, and the number of available capture regions. We find that under certain conditions, the number of cumulative captures increases linearly in time with a slope and duration determined explicitly by the recharge rate of the capture regions. This recharge rate also determines the mean and variance of the clearance time, defined as the time it takes for all particles to leave the domain. Further, we find that while a finite recharge rate will always result in a lower number of captured particles when compared to instantaneous recharging, it can either increase or decrease the amount of variability. Lastly, we extend the model to partially-absorbing traps in order to investigate the dynamics of receptor activation within an idealized synaptic cleft. We find that the width of the domain controls the amount of time that these receptors are activated, while the number of receptors controls the amplitude of activation. Our mathematical results are derived from considering this system in several ways: as a full spatial diffusion process with recharging traps; as a continuous-time Markov process on a discrete state space; and as a system of ODEs in a mean-field approximation.

I. INTRODUCTION

In this work, we investigate the time dynamics of particles diffusing in a domain with a boundary containing traps (Fig. 1A). After capturing a particle, these traps, or capture regions, become reflecting for a transitory recharge time before capturing additional particles (Fig. 1B). The boundary also contains escape regions, where the particles may freely leave the domain. As a result, each particle will eventually be removed from the domain by either escaping or being captured. We are interested in the time evolution of the first and second moments of a) the number of particles remaining in the domain, b) the number of cumulative captures, and c) the number of available capture regions evolve with time. Specifically, we focus on how these time courses are affected by the capture regions having a finite recharge rate.

The study of this stochastic process, referred to here as diffusion with recharging traps (DiRT), is primarily motivated by two applications: 1) molecules interacting with receptors (e.g., neurotransmitters in the synaptic cleft [1] and drug delivery via biodegradable nanoparticles [2]), and 2) prey being ambushed by predators [3]. In both of these applications, the capture regions (receptors/predators) must recharge between captures, and how the number of cumulative captures evolves with time is crucial to understanding the process (when downstream molecules are produced/how long do prey have to escape).

This non-instantaneous recharge rate results in the particles indirectly interacting with each other, resulting in a significantly different problem mathematically than those studied previously. Much work has been done in regards to the distribution of exit times when the particles are trying to find small targets, in what is known as the narrow escape problem [4–7]. These results have also been extended to account for particles that interact directly with one another in the domain (e.g., particles in a highly crowded environment) [8]. We deviate from these previous studies in this work by not necessarily assuming that the capture regions are small, and by having the particles interact via the switching boundary conditions. There has also been a large amount of work completed on studying diffusion with stochastically switching boundary conditions [9–14]. In these studies, the particle paths are also statistically correlated, since they are diffusing in the same random environment. However, the state of

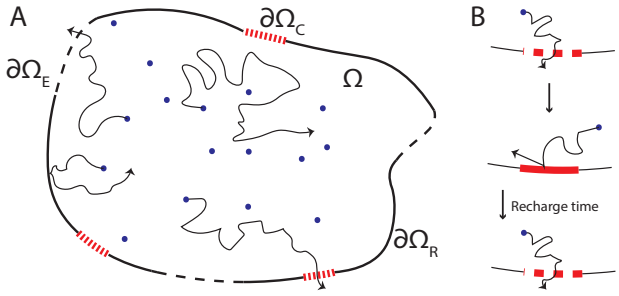

FIG. 1. **Schematics of domain and recharging capture regions.** A: Particles diffusing in domain Ω with boundary $\partial\Omega = \partial\Omega_R \cup \partial\Omega_C \cup \partial\Omega_E$, where $\partial\Omega_R$ are reflecting regions, $\partial\Omega_C$ are capture regions, and $\partial\Omega_E$ are escape regions. B: After capturing a particle, capture regions are reflecting for a transitory recharge time, which we take to be exponentially distributed with rate ρ, where ρ is referred to as the recharge rate.

* borisyuk@math.utah.edu

the boundary does not depend on interacting with the particles, and the particles' paths do not influence one another.

In our previous work, we investigated the average number of total captures in the DiRT process [15]. We proved that this quantity grows logarithmically in the number of initial particles. This result is drastically different from the linear growth that occurs when capture regions recharge instantaneously. However, this previous work offers no information about the time dynamics of the process or higher-order statistics.

In this work, we extend this previous study by investigating the dynamical behavior of not only the number of cumulative captures, but also the number of particles remaining in the domain and the number of available capture regions. We are specifically interested in answering the following questions: What is the role of the recharge rate in determining the mean dynamics? More broadly, what are the overall trends of the dynamical behavior of these higher-order statistics, and how do parameters such as location, number, and recharge of capture regions influence these time courses? Specifically, we seek analytical answers to these questions.

While insight into this problem can be gained with direct Monte Carlo simulations of the DiRT process, such simulations are computationally expensive for a large number of particles. Further, due to the correlations that arise between particles, this spatial and stochastic process is challenging to investigate analytically. Thus, we begin this work by approximating this stochastic process with a continuous-time Markov process on a discrete state space, along with its corresponding mean field approximation and reduction in the limit that captures occur instantly (Section II). These approximations significantly reduce the complexity of the DiRT model and are then used to answer the questions outlined in the previous paragraph (Section III).

II. DIRT MODEL AND APPROXIMATIONS

This work focuses on understanding the underlying stochastic dynamics of the diffusion with recharging traps (DiRT) process, which we define precisely in the next subsection. To yield analytical result pertaining to this model, we derive a series of approximations to the DiRT model that capture similar qualitative and quantitative results, under certain conditions. We first make a quasi-stationary distribution assumption on the distribution of particles to derive a continuous-time Markov process on a discrete state space that is still stochastic, but non-spatial. We then make a mean field approximation to yield a non-spatial and deterministic model. Then, assuming that captures occur instantly, we reduce the discrete state model to yield a non-spatial, stochastic model, which is simplified enough to yield analytical results. Thus, in total, we consider models that take the following forms: (1) spatial and stochastic, (2) non-spatial and stochastic, and (3) non-spatial and deterministic (Fig. 2). With this toolbox of models in hand, we are able to select the appropriate models to answer each of the questions proposed in Section I, yielding insights into the original diffusion with recharging traps process.

A. Diffusion with Recharging Traps

Consider n particles diffusing in a bounded domain $\Omega \subset \mathbb{R}^n$ (Fig. 1A). The boundary ($\partial\Omega$) is partitioned into *escape* regions which absorb particles ($\partial\Omega_E$), reflecting regions which reflect particles ($\partial\Omega_R$), and m-many traps, or *capture* regions ($\partial\Omega_C = \cup_{k=1}^{m} \partial\Omega_C^k$). After capturing a particle, a capture region becomes reflecting for a transitory *recharge* time, where the recharge time is an exponential random variable with rate ρ, during which it cannot capture additional particles (Fig. 1B). The locations of the n molecules diffusing in this domain can be described by the following set of stochastic differential equations

$$d\mathbf{X}_k(t) = \sqrt{2D} d\mathbf{W}_k(t), \quad k = 1, ..., n, \quad \text{for } \mathbf{X}_k(t) \in \Omega, \tag{1}$$

where the $\mathbf{X}_k(t)$ denotes the location of the particle, the $\mathbf{W}_j(t)$'s are independent Wiener processes, and D is the diffusivity. While we assume that these particles do not interact during motion, the boundary conditions depend on the paths of particles, and as a result, the particles can indirectly affect each other. Eventually, all particles will leave the domain either by escaping through an escape region or by being captured by a capture region.

We focus of three key variables: the number of particles remaining in the domain at time t, $P(t)$, the number of captured particles before time t, $C(t)$, and the number of available capture regions at time t, $R(t)$. This paper focuses on understanding the dynamics and statistics of these variables as a function of the number of initial particles n and the recharge rate of the capture regions ρ. We are particularly interested in finite ρ. In the limit $\rho \to \infty$ (instantaneous recharge), the capture regions behave exactly like escape regions, eliminating the correlation between particles paths and allowing the use of more traditional techniques. For example, it is easy to show that the number of total captures follows a binomial distribution with mean nh and variance $nh(1-h)$, where h is the probability of hitting a capture region for a given initial condition. We provide more details about computing h in the Supplementary Materials [16].

B. Continuous-Time Markov Process on Discrete States

While the DiRT model tracks the paths of individual particles, the dynamics of $P(t)$, $C(t)$, and $R(t)$ simply depend on when one of the following events occurs: (i)

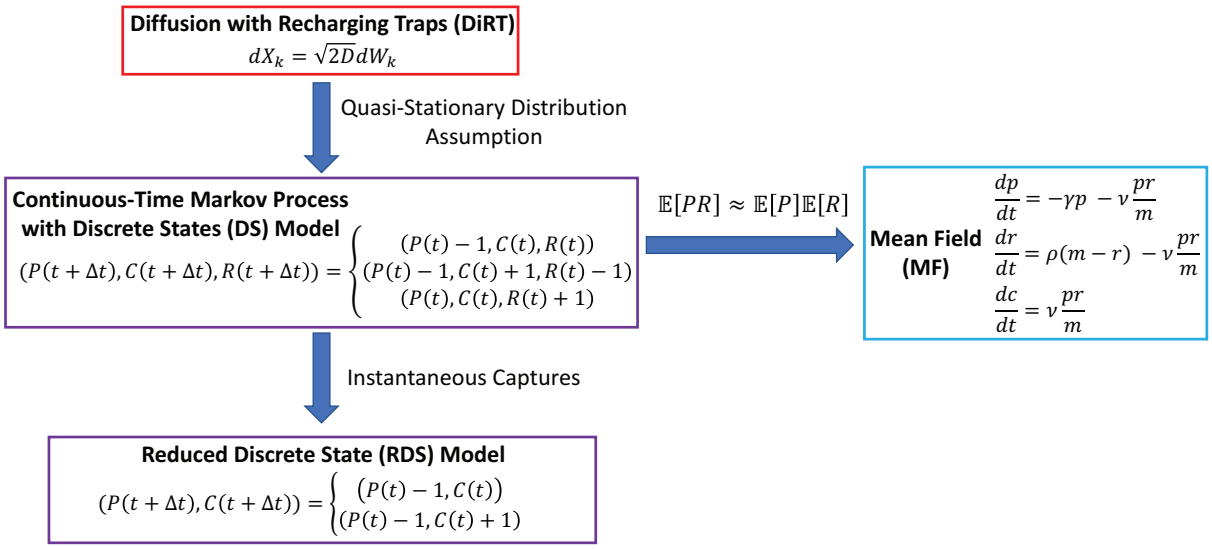

FIG. 2. **Flow diagram of all models.** Red box: DiRT model (spatial and stochastic), Purple box: DS and RDS models (non-spatial and stochastic), and Blue box: MF model (non-spatial and deterministic).

a particle escapes the domain, (ii) a particle is captured and a capture region closes, and (iii) a capture region reopens. Due to this fact, we approximate the DiRT model with a discrete state model, where the states are given by $(P(t), C(t), R(t))$.

Assuming that we are currently in state $(P(t), C(t), R(t))$, there are three possible states it may transition to, namely

$$(P(t)-1, C(t), R(t)), \text{ particle escapes,}$$
$$(P(t)-1, C(t)+1, R(t)-1), \text{ particle is captured,}$$
$$\text{and } (P(t), C(t), R(t)+1), \text{ capture region reopens.}$$

Further, the rates can be estimated from simulations of the DiRT model. For a general transition from discrete state (P, C, R) to $(\widehat{P}, \widehat{C}, \widehat{R})$, there is a corresponding transition rate $\kappa_{pcr,\hat{p}\hat{c}\hat{r}}$, which has the maximum likelihood estimator [17–19]

$$\widehat{\kappa}_{pcr,\hat{p}\hat{c}\hat{r}} = \frac{\#\text{ of transitions from } (P,C,R) \text{ to } (\widehat{P},\widehat{C},\widehat{R})}{\text{total time in state } (P,C,R)}.$$

Unfortunately, there are several drawbacks to using this maximum likelihood estimator in this context. Most notably, the number of states in this model is $\mathcal{O}(n^2 m)$, and each state is visited at most once during a single simulation of the DiRT model. Thus, an unreasonable number of simulations of the DiRT model for a given domain Ω and boundary $\partial\Omega$ are required to get estimates of these transition rates. As a result, it would be easier to use these simulations of the DiRT model directly to understand the time courses of $P(t)$, $C(t)$, and $R(t)$.

With this key drawback in mind, we make the additional approximation that the transition rates are proportional to the number of molecules remaining in the domain and the number of open capture regions. Specifically, the transitions from $(P(t), C(t), R(t))$ are

$$(P(t)-1, C(t), R(t)), \text{ with rate } \gamma P(t),$$
$$(P(t)-1, C(t)+1, R(t)-1), \text{ with rate } \nu P(t)\frac{R(t)}{m},$$
$$\text{and } (P(t), C(t), R(t)+1), \text{ with rate } \rho(m-R(t)),$$

where γ, ν, and ρ are constants independent of the current state, and m is the total number of capture regions. While this approximation significantly reduces the number of parameters, it remains to be shown whether we can choose constants γ and ν such that this discrete state model captures similar quantitative characteristics as the DiRT model (note: ρ is the mean recharge rate for the capture regions).

We make the following assumption for γ and ν: the rate a particle escapes (is captured in) the domain is proportional to the probability of hitting the escape (capture) region and inversely proportional to the average time it takes a particle to reach the escape (capture) region. More specifically, we take these constants to be of the form h/τ_s, where h is the probability of hitting the region of interest and τ_s is the the mean first passage time to hit an absorbing region of the boundary, assuming that the particles are distributed according to a quasi-stationary distribution (QSD). The full algorithm for estimating these parameter values and sufficient conditions for when this approximation may be reasonably accurate can be found in the Supplementary Materials [16].

C. Mean Field Approximation

It is straightforward to write down the corresponding general master equation for our discrete state model. Further, this equation can be used to derive the following exact system of differential equations for $\mathbb{E}[C(t)]$, $\mathbb{E}[P(t)]$, and $\mathbb{E}[R(t)]$ using techniques found in [20],

$$\begin{aligned}\frac{d\mathbb{E}[P]}{dt} &= -\gamma\mathbb{E}[P] - \frac{\nu\mathbb{E}[PR]}{m},\\ \frac{d\mathbb{E}[R]}{dt} &= \rho(m - \mathbb{E}[R]) - \frac{\nu\mathbb{E}[PR]}{m},\\ \frac{d\mathbb{E}[C]}{dt} &= \frac{\nu\mathbb{E}[PR]}{m}.\end{aligned}$$

These techniques can also be used to derive equations for higher-order moments that are necessary to calculate quantities such as variance. For example,

$$\frac{d\mathbb{E}[C^2]}{dt} = \frac{\nu\mathbb{E}[PR]}{m} + \frac{2\nu\mathbb{E}[PRC]}{m}.$$

However, it is readily apparent, due to the appearance of the higher-order term $\mathbb{E}[PRC]$, that this will result in a system of infinitely many differential equations, and an approximation must be used to close the system of equations. A number of such approximations were attempted in order to have a system of equations that contained at least second-order moments, but the errors introduced produced results not consistent with the DiRT model. As a result, we reduce the focus of our mean field model to the three equation system for $\mathbb{E}[C(t)]$, $\mathbb{E}[P(t)]$, and $\mathbb{E}[R(t)]$. The following mean field approximation can be used to close this system of three equations

$$\mathbb{E}[PR] \approx \mathbb{E}[P] \cdot \mathbb{E}[R]. \tag{2}$$

Applying this approximation and the following definitions,

$$p(t) = \mathbb{E}[P], \quad c(t) = \mathbb{E}[C], \quad r(t) = \mathbb{E}[R],$$

we find the following closed system of differential equations

$$\begin{aligned}\frac{dp}{dt} &= -\gamma p - \frac{\nu pr}{m},\\ \frac{dr}{dt} &= \rho(m - r) - \frac{\nu pr}{m},\\ \frac{dc}{dt} &= \frac{\nu pr}{m},\end{aligned}$$

with initial conditions $p(0) = n$, $c(0) = 0$, and $r(0) = m$ (i.e., all capture regions are initially open).

D. Reduced Discrete State Model

In the limit $\nu \to \infty$ (instantaneous capture rate) the discrete state model can be reduced significantly. Specifically, the states are given by $(P(t), C(t))$, with transitions

$$\begin{gathered}(P(t) - 1, C(t)), \text{ with rate } \gamma P(t),\\ \text{and } (P(t) - 1, C(t) + 1), \text{ with rate } \rho m.\end{gathered}$$

In the discrete state model, the particles are correlated through the number of available capture regions, since when one particle is captured, the number of available capture regions decreases by one, making subsequent captures less likely. However, the reduced discrete state model does not contain this correlation, and as a result, can yield analytical results relating to higher-order statistics.

E. Example Domains

A complete algorithm to calculate parameters γ and ν, can be found in the Supplementary Materials [16]. This algorithm can be applied to very general bounded domains Ω with boundary $\partial\Omega = \partial\Omega_R \cup \partial\Omega_E \cup \partial\Omega_C$. Here, we provide the description and parameter values for two domains where these approximations perform well, and will be considered for the rest of this work.

First, we consider the 1D domain

$$\Omega^{1\mathrm{D}} = [0, 1],$$

with an escape region at $x = 0$ and a capture region at $x = 1$. We also consider the 2D domain

$$\Omega^{2\mathrm{D}} = [0, 1] \times [0, 0.1],$$

with escape regions along $x = 0$ and $x = 1$, $\partial\Omega_C = \{(x, y)|y = 0 \text{ and } x \in [0.250, 0.417] \cup [0.417, 0.583] \cup [0.583, 0.750]\}$ ($m = 3$ capture regions), and reflecting boundaries for the rest of the domain (Fig. 3). This rectangular domain, longer in the horizontal direction, was inspired by a synaptic cleft, and used in [15]. Initially, the particles are located at $x = 0.5$ in $\Omega^{1\mathrm{D}}$ and $x = 0.5$, $y = 0.1$ in $\Omega^{2\mathrm{D}}$ (triangle in left panels of Fig. 3). We choose this point distribution in order to avoid biasing our results by making the unreasonable assumption that the particles are initially distributed according to their QSD, which would surely benefit our approximation.

All associated parameter values for these domains can be found in Table I. The first four parameters in this table (those to the left of the double vertical line) were assumed, while those to the right were calculated using the algorithm. For this paper, we consider arbitrary time and space units.

III. RESULTS

With the toolbox of models outlined in Sections II and the details found in the Supplementary Materials [16] to calculate the necessary parameters, we now seek to answer each of the motivating questions outlined in Section I. Specifically, we seek to characterize the time courses of the DiRT process, focusing on the number of particles remaining in the domain, $P(t)$, the number of cumulative captures, $C(t)$, and the number of available capture regions, $R(t)$. Using the discrete state and mean field

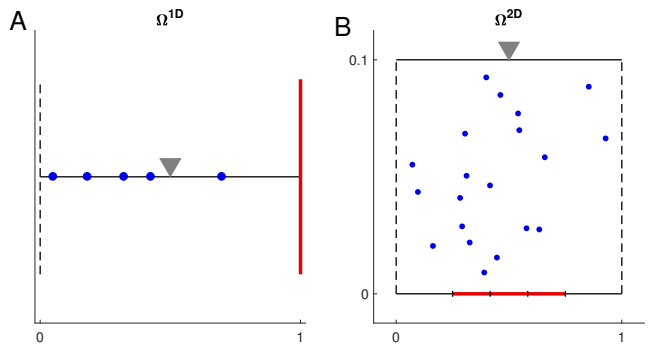

FIG. 3. **Example Domains.** Top: Ω^{1D}, Bottom: Ω^{2D}. The escape regions denoted by black, dashed lines, capture regions by red, solid lines, and reflecting regions by black, solid lines. Unless otherwise specified, all particles are initially located at the gray triangles in each domain for simulations of the DiRT model.

TABLE I. Parameter values for Ω^{1D} and Ω^{2D} (capture regions located along $y = 0$ and $x \in (0.25, 0.75)$). The parameters to the left of the double vertical line were assumed. The remaining parameters, were found following the algorithm provided in the Supplemental Materials [16] (analytically for Ω^{1D} and numerically for Ω^{2D} using the NDEigensystem and NDSolveValue functions in Mathematica [21]). Unless otherwise noted, these are parameters used in the figures. The units are arbitrary time and space units.

	D	n	m	ρ	γ	h	λ_1	$\nu = h \cdot \lambda_1$
Ω^{1D}	1	100	1	10	2.467	0.500	9.870	4.935
Ω^{2D}	1	1000	3	10	9.870	0.563	110.808	62.394

approximations, we examine how these time courses depend explicitly on the recharge rate ρ. We also investigate higher-order statistics (variance and coefficient of variation) of the number of cumulative captures, and how these depend on ρ, as well as the number and distribution of capture regions. Finally, we extend the model to the case of partially-absorbing capture regions.

A. Accuracy of the Discrete State Model

We start by verifying that the discrete state model accurately captures the average behavior of the DiRT model in domains Ω^{1D} and Ω^{2D} (defined in Section II E). We estimate the parameter values to use in the discrete state model via an algorithm outlined in the Supplemental Materials [16]. This calculation assumes a quasi-stationary distribution (QSD) of particles conditioned on not being absorbed for large time. As a result, we expect the approximation of the DiRT process by the discrete state model to be the most accurate when the particle distribution converges quickly to this QSD. We denote this convergence rate by the function $\alpha(\Omega, \partial\Omega, D, \rho)$, where Ω is the domain with boundary $\partial\Omega$, D is the diffusion coefficient and ρ is the recharge rate (see Supplemental Materials [16] for additional details).

We first consider domain Ω^{1D} and compare the $\mathbb{E}[P(t)]$, $\mathbb{E}[C(t)]$, and $\mathbb{E}[R(t)]$ estimated from simulations of both models (Fig. 4). We find qualitative and quantitative similarities with all three variables. More specifically, we see that in both models, the expected number of remaining particles, $\mathbb{E}[P(t)]$, decays exponentially. Meanwhile, the expected number of cumulative captures, $\mathbb{E}[C(t)]$, rises quickly to one (the total number of capture regions in this domain), and then increases linearly, until saturating. Lastly, the expected number of available capture regions, $\mathbb{E}[R(t)]$, quickly drops close to zero, and then increases back to one sigmoidally.

The convergence rate for this domain and parameter values is

$$\alpha(\Omega^{1D}, \partial\Omega^{1D}, 1, 10) \approx 1.97.$$

While this rate is exponential (as discussed in the Supplemental Materials [16]), we find that the distribution of particles is not particularly close to the QSD in the DiRT model when $t \ll 1$ (Fig. 4A, inset). Specifically, we find that $\mathbb{E}[P(t)]$ stays elevated for a moment in the DiRT model before dropping, unlike in the discrete state model. This result is expected, since the particles initially begin at $x = 0.5$ for the DiRT model and are not immediately close to an absorbing region. This inset also notes that once the number of particles in the domain does begin to drop in the DiRT model, it drops at a faster rate than the discrete state model. During this time, the particle distribution has yet to converge to the QSD in the DiRT model, and the escape rate is actually higher than estimated rate. As a result, the discrete state model overestimates $\mathbb{E}[P(t)]$. However, this has a minor effect on $\mathbb{E}[C(t)]$, with the two models resulting in quite similar time courses (Fig. 4B).

We also find great quantitative agreement between the two models for domain Ω^{2D} (Fig. 5). Further, we find similar qualitative time courses as the previous example, namely that $\mathbb{E}[P(t)]$ decays exponentially, $\mathbb{E}[C(t)]$ increases almost instantaneously to three (the total number of capture regions) and then increasing linearly before saturating, and $\mathbb{E}[R(t)]$ drops to zero and saturates back to three sigmoidally.

For this domain and parameter values, the convergence rate is

$$\alpha(\Omega^{2D}, \partial\Omega^{2D}, 1, 10) \approx 2.96,$$

which is larger than in the previous example. Again, the distribution of particles is not particularly close to the QSD during the early moments of $\mathbb{E}[P(t)]$ (Fig. 5A, inset). For the DiRT model, we see a quick decrease of three particles (being absorbed by the three capture regions) and then a slight pause before a sustaining exponential decrease. This result makes sense intuitively. In the DiRT model, the initial distribution of particles

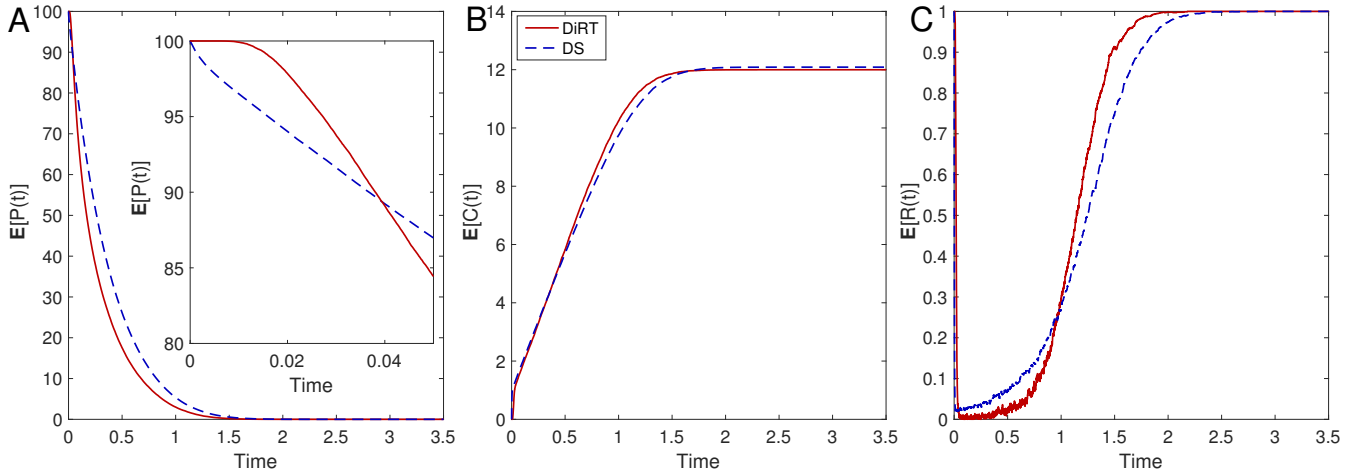

FIG. 4. **Comparison of DiRT and discrete state model for $\Omega^{\mathbf{1D}}$.** A: $\mathbb{E}[P(t)]$, B: $\mathbb{E}[C(t)]$, and C: $\mathbb{E}[R(t)]$ for DiRT (red, solid) and discrete state (blue, dashed) models. Inset shows a zoomed in view of $\mathbb{E}[P(t)]$ for an early time interval. These panels show good agreement between the two models, with the differences arising due to the time it takes for the distribution of particles to converge to the QSD. Parameter values are found in Table I.

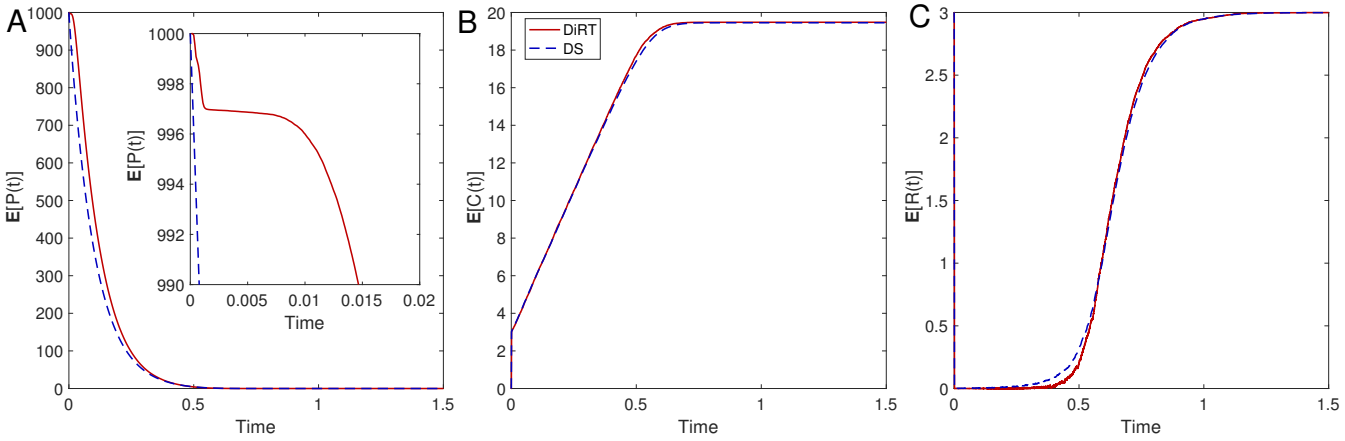

FIG. 5. **Comparison of DiRT and discrete state model for $\Omega^{\mathbf{2D}}$.** A: $\mathbb{E}[P(t)]$, B: $\mathbb{E}[C(t)]$, and C: $\mathbb{E}[R(t)]$ for the DiRT (red, solid) and discrete state (blue, dashed) models. Inset shows a zoomed in view of $\mathbb{E}[P(t)]$ at an early time. Similar to the previous figure, we again see good agreement between the two models, with the differences arising due to the time it takes for the distribution of particles to converge to the QSD. Parameter values are found in Table I.

is $\delta(x-0.5)\delta(y-0.1)$, and the particles are much closer to the capture regions than the escape regions. Similar to the last example, this transient state is not captured in simulations of the discrete state model, as expected. However, again, despite a noticeable difference in the time course of $\mathbb{E}[P(t)]$ (here, the discrete state model results in an underestimation), we see a great agreement for $\mathbb{E}[C(t)]$ and $\mathbb{E}[R(t)]$.

For the rest of this article, we limit ourselves to domain Ω^{2D}, where we have shown that this approximation performs well. Unless otherwise noted, the shape of the domain and the number of receptors is the same as those outlined in Subsection II E.

B. Time Course of the Average Behavior

Having established that the discrete state model performs well in capturing the dynamics of the DiRT model, we now turn our attention to understanding the underlying dynamical structure driving the time courses of $\mathbb{E}[P(t)]$, $\mathbb{E}[C(t)]$, and $\mathbb{E}[R(t)]$. To perform this analysis, we employ the deterministic mean field model,

$$\begin{aligned}\frac{dp}{dt} &= -\gamma p - \frac{\nu p r}{m},\\ \frac{dr}{dt} &= \rho(m-r) - \frac{\nu p r}{m},\\ \frac{dc}{dt} &= \frac{\nu p r}{m},\end{aligned}$$

which lends itself well to phase plane analysis.

1. Accuracy of the Mean Field Approximation

Before investigating the mean field model in detail, we first assess its accuracy, since the mean field approximation, Eq. (2), is only exact when P and R are uncorrelated. This is certainly not the case here, since when a particle binds to a capture region and decreases R, it has also been removed from the domain, decreasing P. However, despite this fact, Fig. 6 illustrates that this is not a poor approximation to make. As this figure shows, the discrete state model and the numerical solution to the mean field model quantitatively agree for $\mathbb{E}[P(t)]$, $\mathbb{E}[C(t)]$, and $\mathbb{E}[R(t)]$. Further, the inset of Fig. 6A shows that the absolute error of the mean field approximation, (i.e., $|\mathbb{E}[PR] - \mathbb{E}[P] \cdot \mathbb{E}[R]|$) is small, and only increases to a potentially significant level when a few particles are remaining in the domain (which only occurs for a short period of time).

2. Phase Plane Analysis of Mean Field System

Since the mean field model accurately captures the dynamics observed in the discrete state model, it can be used to understand the mean dynamics of the original spatial and stochastic DiRT process. Specifically, we turn our attention to the time course of $c(t)$, where we have seen previously that it increases almost instantaneously to the number of capture regions and then grows linearly before saturating. Specifically, one can show (Supplemental Material [16]) that for a large portion of time

$$\frac{dc}{dt} \approx m\rho.$$

This result matches the slope of $c(t)$ during its linear growth regime in the DiRT and discrete state models. In words, $m\rho$ is the rate that particles are captured by all capture regions, assuming they each capture a particle the moment they have recharged. Further, the duration of this linear growth is given by

$$T^{\text{linear}} = \frac{1}{\gamma} \log\left(\frac{1 + \frac{m\rho}{n\gamma}}{C + \frac{m\rho}{n\gamma}}\right), \tag{3}$$

where C is the fraction of particles remaining at time T^{linear}. A plot of Eq. (3) as a function of recharge rate ρ for various values of C is found in Fig. 7. This figure illustrates that T^{linear} monotonically decreases as a function of ρ. The dashed portion of line indicates the parameter regime where $T^{\text{linear}} > 1/(m\rho)$, meaning the predicted time is greater than the average recharge rate of the receptors; therefore, we do not expect to observe this linear growth. For example, when $\rho = 0.01$ and $C = 0.01$, the equation finds that $T^{\text{linear}} = 0.47$. However, with this choice of ρ, the average time for a capture region to recharge is $1/(3 \cdot 0.01)$ or approximately 33.33. Not only is this recharge rate greater than T^{linear}, but it is greater than the expected amount of time of particle clearance (i.e., the time the last particle leaves the domain). Combining this with the fact that $T^{\text{linear}} \to 0$ for large values of ρ, we conclude that Eq. (3) is most useful for intermediate values of ρ (i.e., between these two extremes). Unfortunately, we also note that in this regime, the curves are sensitive to the parameter C, which is domain dependent. Again, while choosing $C > 0$ might yield more accurate results in given domain, choosing $C = 0$ provides a reasonable upper bound.

This result may be particularly helpful for understanding applications where multiple puffs of particles are inserted in the domain over a period of time (e.g., neuronal synapses), and can provide a bound on the time between puff events such that particles in different puffs minimally interact. This is investigated in more detail in the next section, where we examine the statistics of the clearance time.

C. Higher-order Statistics for Total Particle Captures and Clearance Time

Having investigated the dynamics of $\mathbb{E}[P(t)]$, $\mathbb{E}[C(t)]$, and $\mathbb{E}[R(t)]$, and explored the phase space underlying $\mathbb{E}[C(t)]$ in detail, we now seek information regarding higher-order statistics. Focusing first on deriving analytical results, we turn to the reduced discrete state model.

1. Estimating the Total Average Number of Captures and its Variance

Considering first the average number of total captures, one can show (Supplemental Material [16]) that

$$\Rightarrow \mathbb{E}[\mathcal{C}_{\text{total}}] = m + \frac{m\rho}{\gamma}\left[\Psi^{(0)}\left(n - m + 1 + m\rho/\gamma\right) - \Psi^{(0)}\left(1 + m\rho/\gamma\right)\right], \tag{4}$$

$$\text{var}[\mathcal{C}_{\text{total}}] = \frac{m\rho}{\gamma}\left[\Psi^{(0)}\left(n - m + 1 + m\rho/\gamma\right) - \Psi^{(0)}\left(1 + m\rho/\gamma\right)\right] + \left(\frac{m\rho}{\gamma}\right)^2\left[\Psi^{(1)}\left(n - m + 1 + m\rho/\gamma\right) - \Psi^{(1)}\left(1 + m\rho/\gamma\right)\right], \tag{5}$$

where $\Psi^{(j)}$ is the polygamma function of order j [22]. Although Eqs. (4) and (5) appear unwieldy, they provide valuable insight as $n \to \infty$ when coupled with asymptotic

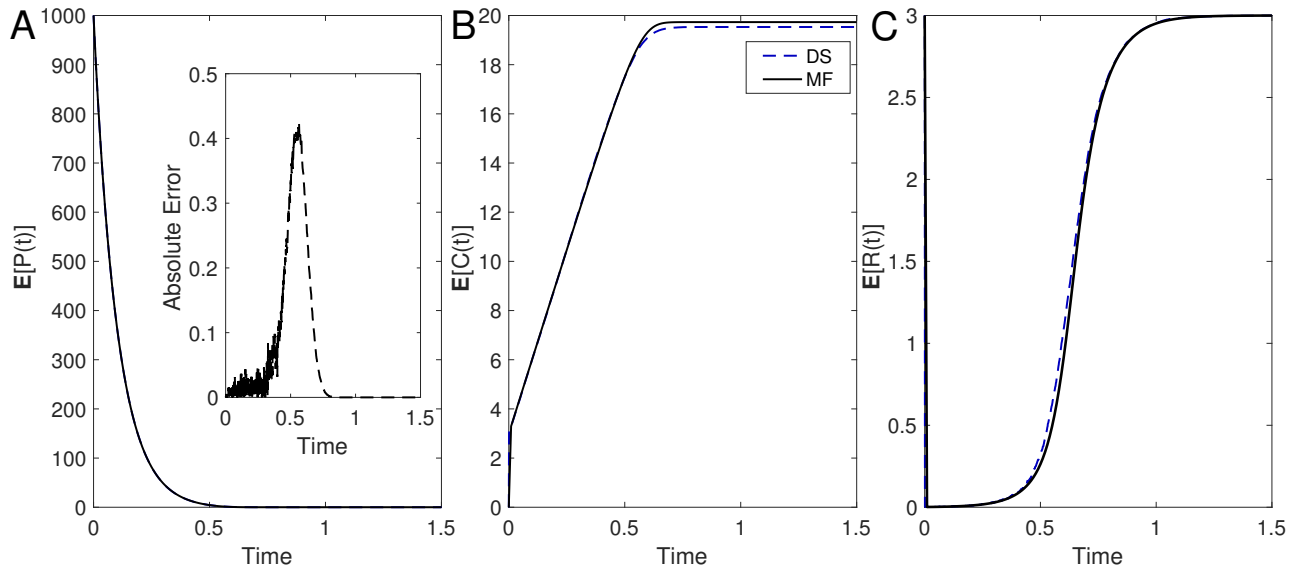

FIG. 6. **Comparing the discrete state and mean field models.** A: $\mathbb{E}[P(t)]$, B: $\mathbb{E}[C(t)]$, and C: $\mathbb{E}[R(t)]$ for the discrete state (blue, dashed) and mean field (black, solid) models. Inset shows a zoomed the error in the mean field approximation $|\mathbb{E}[PR] - \mathbb{E}[P]\cdot\mathbb{E}[R]|$. Panels show great agreement between the two models. Simulations were ran in domain Ω^{2D} (parameters found in Table I).

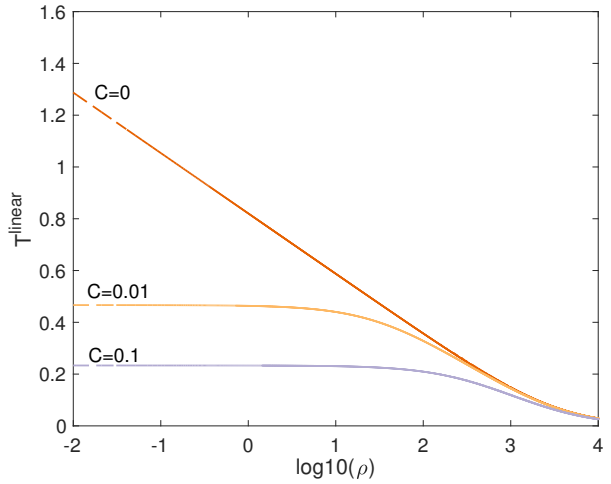

FIG. 7. Plot of the duration of linear growth (Eq. (3)), for different values of C, using parameters from Ω^{2D} (Table I). The dashed portion of the line denotes when $T^{\text{linear}} > 1/(m\rho)$, the average time for a capture region to recharge. This figure shows that the linear growth phase is most prominent for intermediate values of ρ.

expansions for $\Psi^{(0)}(n)$ and $\Psi^{(1)}(n)$, namely

$$\mathbb{E}[\mathcal{C}_{\text{total}}] = m + \frac{m\rho}{\gamma}\log n - \frac{m\rho}{\gamma}\Psi^{(0)}(1+m\rho/\gamma) + \mathcal{O}\left(\frac{1}{n}\right), \tag{6}$$

$$\text{var}[\mathcal{C}_{\text{total}}] = \frac{m\rho}{\gamma}\log n - \frac{m\rho}{\gamma}\Psi^{(0)}(1+m\rho/\gamma) - \left(\frac{m\rho}{\gamma}\right)^2\Psi^{(1)}(1+m\rho/\gamma) + \mathcal{O}\left(\frac{1}{n}\right). \tag{7}$$

Thus, in agreement with our previous results, the mean grows like $\mathcal{O}(\log n)$ [15]. Further, this calculation suggests the new result that the variance should also grow like $\mathcal{O}(\log n)$. Fig. 8A compares this theoretical result to simulations from the DiRT model, and finds that not only does the variance estimated from DiRT model grow like $\mathcal{O}(\log n)$, but it matches well with Eq. (5). We can also use these theoretical results to approximate how the coefficient of variation, a normalized measure of variance,

$$c_v = \frac{\text{standard deviation}}{\text{mean}},$$

changes with n, and find that it decays as $\mathcal{O}(1/\sqrt{\log n})$.

We can compare these results to those when the capture regions recharge instantaneously. In that case, recall that the number of total captures follows a binomial distribution, with n trials and probability of success h; therefore, the expected number of particles captured is nh and has a variance of $nh(1-h)$, both of which grow as $\mathcal{O}(n)$. Further, in the instantaneous recharge case, the c_v grows as $\mathcal{O}(1/\sqrt{n})$. As a result, it appears that a finite recharge rate has the effect of decreasing the rate

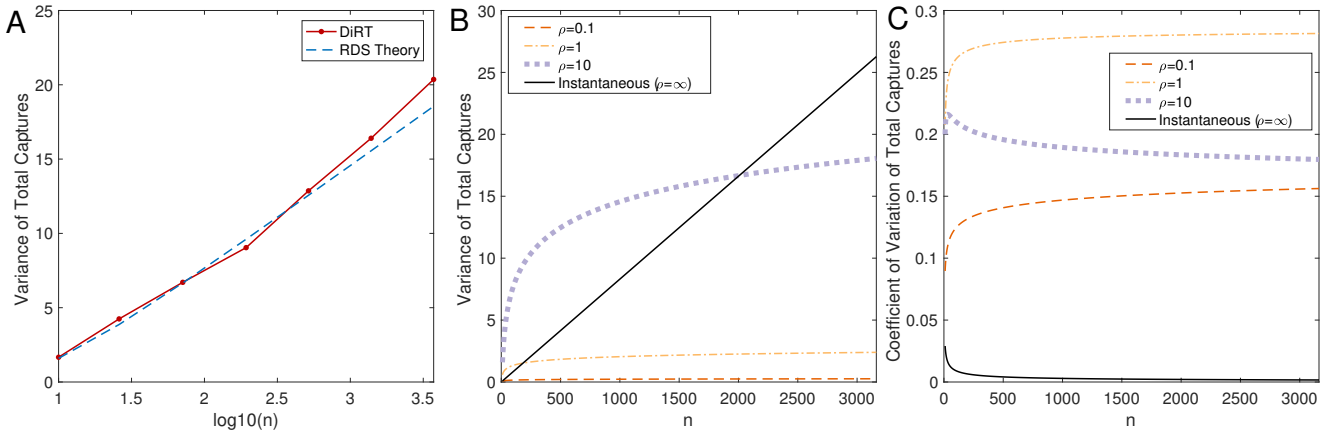

FIG. 8. **Variability of Total Captures.** A) The variance of total captures from the DiRT model (red, dotted-solid) matches well with Eq. (5) (blue, dashed) for Ω^{2D} with $\rho = 10$. B) The variance and C) the coefficient of variation of total captures as a function of n from Eq. (5) for different recharge rates (dashed, dotted, and dot-dashed) and with instantaneous recharge (solid, $h = 0.99$) in Ω^{2D}. Depending on parameters, a finite recharge rate may lead to more or less variability when compare to an instantaneous recharge rate.

at which the expected value and variance terms grow as a function of n, while in terms of this normalized measure of variability, a finite recharge rate has the ability to increase the amount of variability observed.

However, this asymptotic analysis is true only in the limit $n \to \infty$. For finite n, we directly compare Eq. (5) to $nh(1-h)$ for parameters from domain Ω^{2D} ($h = 0.99$ for this domain and initial condition). As Fig. 8B illustrates, while Eq. (5) (dashed) grows as $\mathcal{O}(\log(n))$ for different values of ρ and the instantaneous recharge (black, solid) case grows as $\mathcal{O}(n)$, it is not necessarily true that a finite recharge rate will lead to a lower variance. Specifically, we see that while the curve for $\rho = 0.1$ lies below the solid line, this is not the case for $\rho = 1$ and 10 for all values of n.

We can understand this result by noting that in the limit $\rho \to 0$, each capture region will catch at most one particle, with all remaining particles almost surely escaping the domain before they have a chance to recharge. As a result, there is little to no variability for $\rho \ll 1$; thus increasing ρ will lead to an increase in variability. The fact that the $\rho = 1$ and $\rho = 10$ curves lie above the instantaneous recharge curve for some values of n is a result of the large hitting probability used in the $nh(1-h)$ calculation, resulting in a small slope for this line. As a result, we conclude that a finite recharge rate can result in a higher variance for the total number of captures, but this result depends on the domain, initial condition, n, and ρ.

In terms of the coefficient of variation, the results are more straightforward, with Fig. 8C showing that a finite recharge rate does consistently result in a higher coefficient of variation when compared to $\rho = \infty$. However, it does not behave monotonically as a function of ρ ($\rho = 0.1$ has the lowest c_v, $\rho = 1$ the highest, and $\rho = 10$ rests in the middle). The coefficient of variation as a function of time is explored in more detail in Subsection III D.

Equations 4 and 5 can also be used directly to predict and compare the amount of variability of two neuronal synapses expressing different types of receptors. Specifically, we consider the synapses discussed in [15], with one containing exclusively NMDA receptors (slow recharge rate) and another consisting of AMPA receptors (fast recharge rate). We find that the variability in the total number of captures for these two synapses to be drastically different ($\text{var}[\mathcal{C}_{\text{total}}] = 0.20$ for the NMDA synapse and 47.77 for the AMPA synapse). However, this is not particularly surprising, since synapses with AMPA receptors have a much higher mean number of particle captures (due to both the larger number of receptors, 20 NMDA vs. 200 AMPA receptors, and the faster recharge). We can account for this disparity by comparing instead the coefficients of variations. Doing so still yields a noticeable difference between the two cases (0.01 for the NMDA synapse and 0.19 for the AMPA synapse). As a result, the synapses with larger fraction of AMPA receptors, are predicted to be more noisy, i.e. result in a less consistent conductance change in the postsynaptic neuron and, subsequently, more neuron response variability and altered information processing in networks with such synapses.

2. *Estimating the Clearance Time*

One can also use the reduced discrete state model to estimate statistics regarding the time it takes for all particles to leave the domain, referred to here as the clearance time. Let T^{clear} denote this random variable and let T_k denote the interleaving time between the $(k-1)$th

particle and kth particle. It follows that

$$T^{\text{clear}} = \sum_{k=m+1}^{n} T_k,$$

where T_k is simply an exponential random variable with parameter $m\rho+\gamma(n-(k-1))$. As a result, we can perform a very similar calculation as the one in Subsection III C 1 to find $\mathbb{E}[T^{\text{clear}}]$ and $\text{var}[T^{\text{clear}}]$,

$$\mathbb{E}[T^{\text{clear}}] = \frac{1}{\gamma}\left[\Psi^{(0)}(n-m+1+m\rho/\gamma) - \Psi^{(0)}(1+m\rho/\gamma)\right], \tag{8}$$

$$\text{var}[T^{\text{clear}}] = \frac{1}{\gamma^2}\left[-\Psi^{(1)}(n-m+1+m\rho/\gamma) + \Psi^{(1)}(1+m\rho/\gamma)\right]. \tag{9}$$

Using the asymptotic expansions from the previous section, it follows that the expected value of the clearance time grows as $\mathcal{O}(\log n)$, while the variance grows as $\mathcal{O}(1)$. This is illustrated in Fig. 9, where for a fixed recharge rate ρ, the bars denoting one standard deviation remain relatively unchanged. Interestingly, as the recharge rate increases, not only does the expected clearance time decrease, but the variability also decreases.

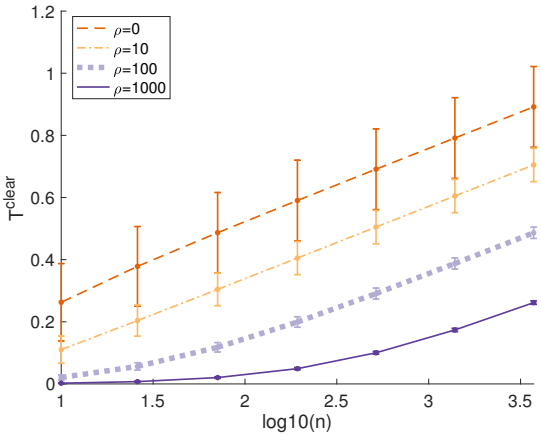

FIG. 9. Comparing the expected value and variance of clearance times for different values of ρ using equations Eqs. (8) and (9). The bars denote one standard deviation. We find that ρ determines the mean and variance of the random variable T^{clear}. Other parameters can be found in Table I for Ω^{2D}.

We can again return to the neuronal example and compare the clearance time of neurotransmitters for the two types of synapses. Using Equation 8 we find that for the NMDA synapse, the clearance time is 0.11 ms and is 0.07 ms for the AMPA synapse. This minimal discrepancy suggests that the difference in recharge rate between these two types of receptors has a minimal effect on clearance time, and other parameters of the problem (e.g., domain size) have a larger impact. This is examined in more detail in Subsection III E.

D. Dynamics of Higher-order Statistics and Dependence on Parameter Space

Seeking to extend the analytical results from the previous subsection, we now turn our attention to the dynamics of higher-ordered statistics, as well as how results may differ over a wide-range of parameter values. Numerical simulations of the discrete state model is the approach of choice here, by striking a balance between being sufficiently detailed yet computationally tractable.

1. *Time Evolution of the Coefficient of Variation and Dependence on Recharge*

Before exploring the parameter space with the discrete state model, we must first confirm that it accurately matches the higher-order statistics of the DiRT model, since Subsection III A only examined the average behavior. Figs. 10A and 10B compares $c_v(C(t))$ for these two models in Ω^{2D} for different recharge rates. These figures illustrate quantitative agreement for both parameter choices. Further, we observe that for a large recharge rate ($\rho = 1000$), the coefficient of variance decreases monotonically over time, while for a smaller recharge rate ($\rho = 10$), it varies non-monotonically.

Having established this quantitative match between the discrete state and DiRT models, and having found this interesting non-monotonic behavior, we now investigate $c_v(C(t))$ over a wider range of values for ρ using just the discrete state model. As illustrated in Fig. 10C, we find that the final amount of variation (i.e. $\lim_{t\to\infty} c_v(C(t))$) does not vary monotonically with ρ, further confirming our results from Subsection III C 1. Also, this panel indicates that the non-monotonic behavior in time observed in Fig. 10A appears to be an intermediate step between the extremes of a slow and fast recharge rate. For ρ small, the coefficient of variation monotonically increases with time. However, as ρ increases to intermediate values, the coefficient of variation behaves non-monotonically. Specifically, it increases before decreasing to a final value. Interestingly, in the cases where this non-monotonic behavior is observed, $c_v(C(t))$ seems to always peak at the same value. Finally, as ρ increases to larger values, $c_v(C(t))$ monotonically decreases. Thus, a finite recharge rate will not only influence the final amount of variability observed, but the time course of variability.

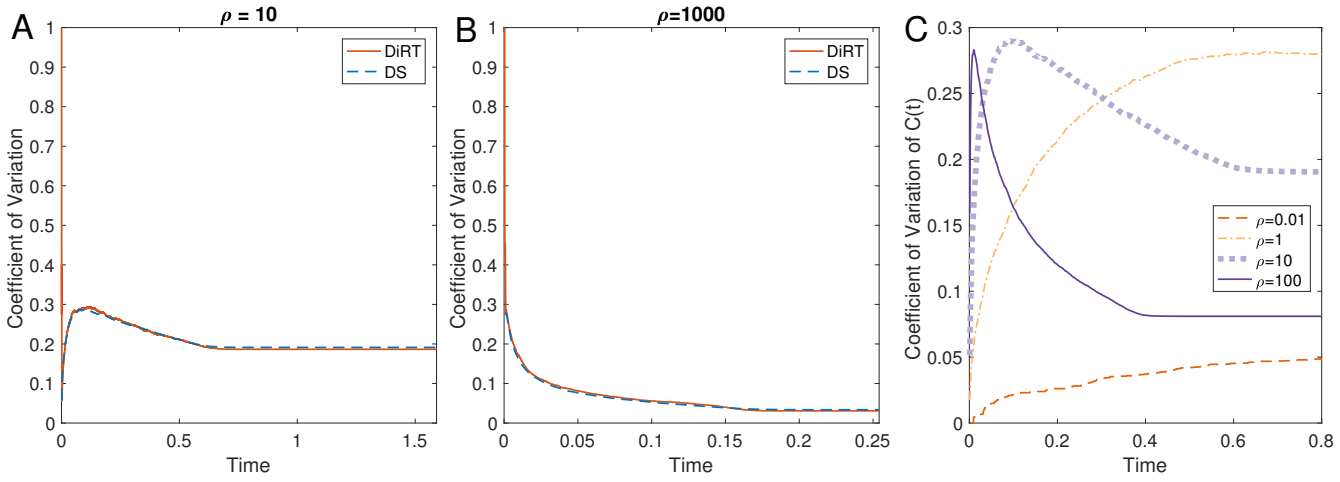

FIG. 10. **Coefficient of Variation of $C(t)$ for the DiRT and discrete state models.** A. $\rho = 10$, B: $\rho = 1000$ for the DiRT (red, solid) and discrete state (blue, dashed) models. Panels shows excellent agreement between the two models. C: Coefficient of Variation of $C(t)$ for the discrete state model as a function of ρ. Panel shows that the c_v varies non-monotonically over time. Simulations were conducted in Ω^{2D} and parameter values can be found in Table I.

2. *Influence of the Number and Spatial Arrangement of Capture Regions*

We now expand our investigation to include the dynamics of the number of available capture regions, and how their number and spatial distribution influence these dynamics. We start by considering Ω^{2D} with one capture region located at $\partial\Omega_c = \{(x, y)|y = 0 \text{ and } x \in [0.45, 0.55]\}$ (Fig. 11, red, dashed). We compare this to the same domain, but with $\partial\Omega_c$ split into five capture regions of equal size (orange, solid). Note that ν and γ are the same for both domains, and their estimation only needs to be performed once. As illustrated in Figs. 11A and 11B, the domain with five capture regions captures more particles, while having a lower amount of variation. Figs. 11C and 11D contain plots for the expected fraction and standard deviation of open capture regions (i.e. $\mathbb{E}[R(t)/m]$), and illustrate that the system reaches steady state faster with five capture regions and has a lower amount of variation for the fraction of open capture regions.

With these results in mind, one might wonder whether having five capture regions yields similar results as having a single capture region with a five times faster recharge rate (purple, dot-dashed). However, Fig. 11 clearly illustrates that this is not the case. The number of cumulative captures does increase, but unlike in the case of five capture regions, the initial increase in $\mathbb{E}[C(t)]$ is only one, as opposed to five. Further, the amount of variation seen is drastically different, and the system returns to steady state significantly faster with this larger recharge rate.

Lastly, we investigate how the spread of capture regions may affect these curves. Specifically, we distributed the five capture regions along $y = 0$, with $\partial\Omega_C = \{(x, y)|y = 0 \text{ and } x \in [0.09, 0.11] \cup [0.29, 0.31] \cup [0.49, 0.51] \cup [0.69, 0.71] \cup [0.89, 0.91]\}$ (purple, dotted). We found a minimum difference between this arrangement of capture regions, and the arrangement where all of the capture regions were placed in the center of the domain. These results suggest that a combination of the number and recharge rate, but not the spatial location of receptors, primarily determines the time courses and their variability. This result is particularly interesting in the context of our neuronal synapse application, where receptors have been shown to cluster in the center of the post-synaptic terminal [23]. Our result suggests that this spatial arrangement of receptors does not directly affect the reliability of signal propagation through the synapse, and the functional consequences of such an arrangement lie elsewhere.

E. Application to an Idealized Synapse

We now apply our mathematical model to investigate the dynamics of an idealized synaptic cleft, where the particles are neurotransmitters, the capture regions are receptors, and the neurotransmitters are broken down by enzymes after being captured by the receptors. In this context, the number of currently bound capture regions (i.e., $m - \mathbb{E}[R(t)]$) is the key variable of interest, as it represents the number of currently activated receptors and relates to the conductance through the post-synaptic neuron. These receptors are not perfect absorbers, leading us to generalize the model to partially-absorbing capture regions. Unlike the perfect absorbing capture regions considered up to this point, there is some probability of a particle not being captured after coming in contact with a partially-absorbing capture region. We can extend the technique used to estimate parameters γ and ν to account for such capture regions by including appropriate Robin boundary conditions (Supplemental Materi-

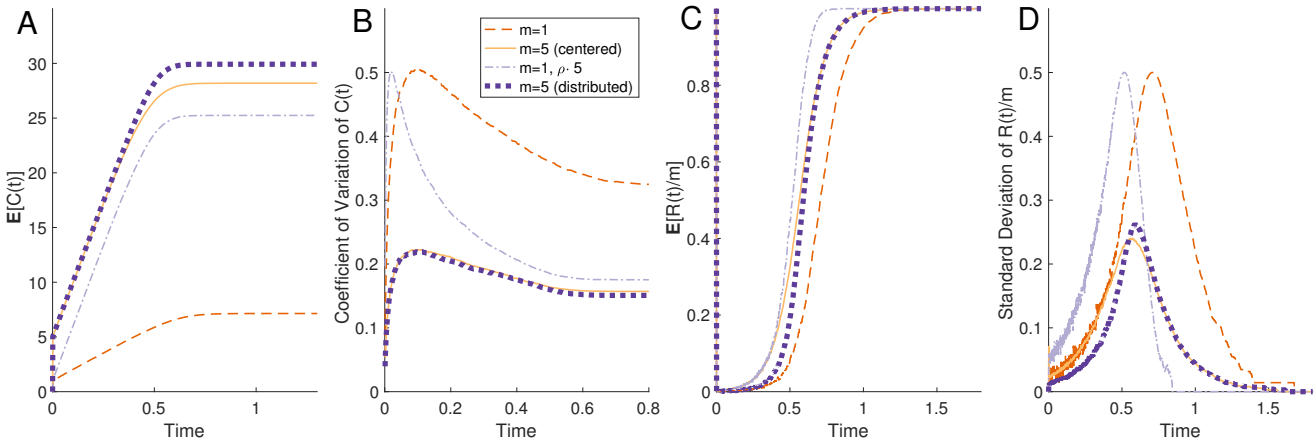

FIG. 11. **Parameter exploration using the discrete state model.** A: $\mathbb{E}[C(t)]$, B: coefficient of variation of $\mathbb{E}[C(t)]$, C: $\mathbb{E}[R(t)/m]$, and D: standard deviation of $R(t)/m$ for different recharge rates, capture region numbers and capture region locations. The domain for all curves is Ω^{2D}. The capture regions have been adjusted to be $\partial\Omega_C = \{(x,y)|y = 0 \text{ and } x \in \cup[0.45, 0.55]\}$ for the $m = 1$ curves, $\partial\Omega_C = \{(x,y)|y = 0 \text{ and } x \in [0.45, 0.47] \cup [047, 0.49] \cup [0.49, 0.51] \cup [0.51, 0.53] \cup [0.53, 0.55]\}$ for the centered $m = 5$ curve, and $\partial\Omega_C = \{(x,y)|y = 0 \text{ and } x \in [0.09, 0.11] \cup [0.29, 0.31] \cup [0.49, 0.51] \cup [0.69, 0.71] \cup [0.89, 0.91]\}$ for the distributed $m = 5$ curve. The algorithm provided in the Supplemental Materials [16] was used to calculate parameters ν and γ.

als [16]). Here, we consider an absorption rate $K = 1$ (in the case of a perfect absorber, $K = \infty$). We also increase the number of capture regions from $m = 3$ to $m = 50$ (still uniformly spaced along the interval $x \in [0.25, 0.75]$), which is closer to reality for a neuronal synapse [24].

Fig. 12A starts the investigation by first illustrating that the discrete state model accurately models the DiRT process with such a partial absorbing capture region (red, solid and blue, dashed). This figure also compares partially-absorbing capture regions (blue, dashed) with perfect absorbers (purple, dot-dashed). These curves show that perfectly absorbing capture regions are faster at capturing particles, they are closer to being fully saturated when $m - \mathbb{E}[R(t)]$ is at its peak, and have a slower initial decay away from this peak.

Returning our attention to the specific application of a neuronal synapse, we investigate how the size of the cleft and number of capture regions influence the time course of $m - \mathbb{E}[R(t)]$, since both of these quantities have been experimentally shown to vary [25, 26]. We first compare Ω^{2D} to the smaller domain $\widehat{\Omega}^{2D}$ (Fig. 12B, inset). As Fig. 12B, illustrates, the magnitude of $m - \mathbb{E}[R(t)]$ does not change between the two domains, but it has a significantly shorter duration in domain $\widehat{\Omega}^{2D}$. We also consider $m = 50$ and $m = 25$ capture regions in domain Ω^{2D} (Fig. 12C). Unsurprisingly, more capture regions are occupied in the $m = 50$ case. However, while the duration of the two curves are similar, the time course with $m = 50$ has a noticeably quicker decay from its maximal value. As a result, we conclude that the discrete state model can approximate a neuronal synapse with partially-absorbing receptors, and finds that the size of the synapse and number of receptors determines the time course of receptor activation.

IV. CONCLUSIONS AND DISCUSSION

In this paper, we investigated the dynamics of the diffusion with recharging traps process, focusing on $P(t)$, the number of particles remaining in the domain, $C(t)$, the number of cumulative captures, and $R(t)$, the number of available capture regions. We outlined conditions where this spatial and stochastic process can be approximated by a discrete state model, and its corresponding mean field approximation. Using these models, we found that the recharge rate, ρ, of the capture regions determines the time course of $\mathbb{E}[C(t)]$ (increases linearly with a slope and duration that explicitly depend on ρ), as well as the average and variance of the clearance time, the time it takes for all particles to leave the domain. In our previous work, we showed that accounting for a finite recharge rate for the capture regions drastically decreased the average number of particles captured when compared to an instantaneous rate [15]. Here, we have built upon that result, and found that, depending on the parameter regime, a finite recharge rate will either increase or decrease the amount of variability. Lastly, we considered the dynamics of the model with partially-absorbing and found that the time course of capture region activation is determined by both the size of the domain and the number of capture regions.

We now mention a couple of possible extensions to the model. First, we note that the continuous-time Markov process on a discrete state space used to approximate the DiRT model consisted of transition rates that only accounted for the number of available capture regions. However, this discrete state model can be made more complex by explicitly accounting for the arrangement of currently available capture regions. For example, with

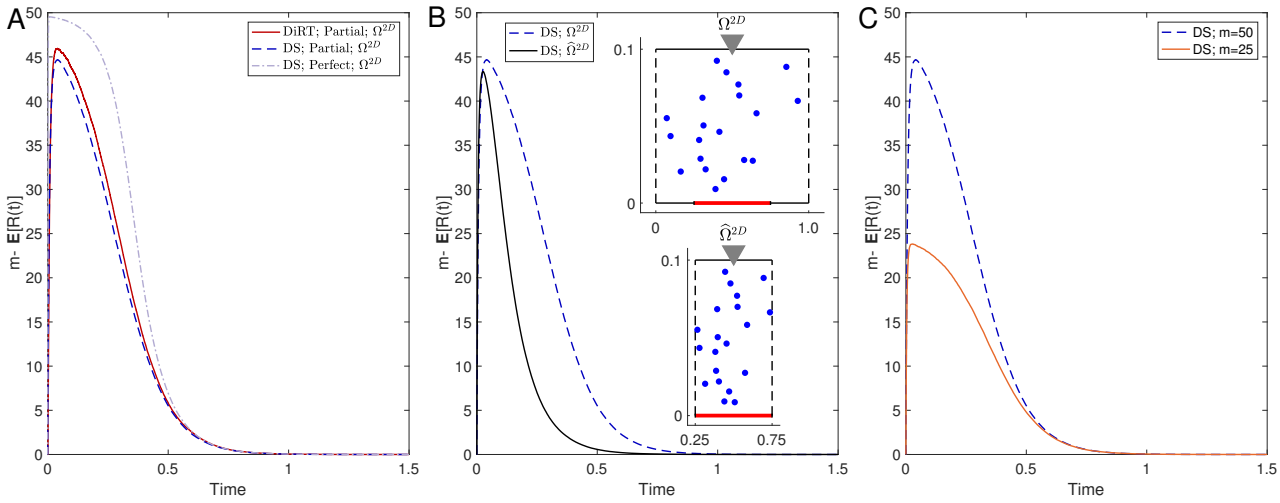

FIG. 12. **Role of domain size and number of capture regions with partially-absorbing capture regions.** A) The average number of occupied capture regions for the DiRT (red, solid) and discrete state (blue, dashed) models for $m = 50$ and partially-absorbing receptors ($K = 1$). The purple, dot-dashed line corresponds to the discrete state model for $m = 50$ and perfect absorbers (parameters found in Table I). B) The average number of occupied capture regions for the discrete state model in domain Ω^{2D} (blue, dashed), and $\widehat{\Omega}^{2D} = [0.25, 0.75] \times [0, 0.1]$ (black, solid) for $m = 50$. C) The average number of occupied capture regions for the discrete state model with $m = 50$ (blue, dashed), and $m = 25$ (orange, solid) capture regions. Parameters γ and ν were calculated using the extensions to the main algorithm and can be found in the Supplemental Materials [16]. For Ω^{2D}: $\gamma = 9.8696$, $\nu = 6.6496$, and for $\widehat{\Omega}^{2D}$: $\gamma = 39.4784$, $\nu = 9.6754$.

$m = 3$ capture regions, we would have escape rates γ_{ijk} and capture rates ν_{ijk}, where i, j, and k denote the state of capture regions one, two, and three respectively (1 if it is available, and 0 otherwise). With this setup, the number of transition rates is $m!$, which is large for even a moderate number of receptors. While this complication to the model would potentially improve the approximation, we have shown that this additional computation was not necessary for a quantitative agreement between the DiRT model and its approximations for domains Ω^{1D} and Ω^{2D}.

One also could generalize the DiRT model to account for more general assumptions on particle motion. Such a generalization would appear in the Fokker-Planck equation, and the algorithm used to calculate the parameters could be extended appropriately. Another possible generalization is to suppose that each particle is removed from the system at some constant rate, γ_{dec} (i.e., particles have an exponentially distributed lifetime, and would apply to second messenger proteins such as IP_3 [27]). In this case, the transition rate for a particle to escape in the discrete state model would simply become $\gamma + \gamma_{\text{dec}}$. Lastly, one could allow for multiple types of capture regions, some that remove the particles from the domain, as we studied here, and others that would return them back into the domain. This would lead to a less-idealized synaptic cleft model, but we note that while this updated model would further reduce the number of molecules seen by the receptors, it would not affect their activation directly.

[1] A. Deutch, "Fundamental neuroscience," (Elsevier Inc., 225 Wyman Street, Waltham, MA 02451, USA, 2013) Chap. 6, pp. 117–138, 4th ed.
[2] A. Kumari, S. K. Yadav, and S. C. Yadav, Colloids Surfaces B Biointerfaces **75**, 1 (2010), arXiv:S0168-3659(00)00339-4.
[3] M. S. DeVries, E. A. K. Murphy, and S. N. Patek, Journal of Experimental Biology **215**, 4374 (2012).
[4] A. Schuss, Z. Singer and D. Holcman, PNAS **104**, 16098 (2007).
[5] O. Bénichou and R. Voituriez, Physics Reports **539**, 225 (2014).
[6] D. Holcman and Z. Schuss, SIAM Rev. **56**, 213 (2014).
[7] S. Ro and Y. Kim, Phys. Rev. E **96** (2017).
[8] T. Agranov and B. Meerson, Phys. Rev. Lett. **120** (2018).
[9] S. D. Lawley, J. C. Mattingly, and M. C. Reed, SIAM J. Math. Anal. **47**, 3035 (2015).
[10] P. C. Bressloff and S. D. Lawley, J. Phys. A **48** (2015), 10.1088/1751-8113/48/10/105001.
[11] S. D. Lawley, SIAM J. Appl. Dyn. Syst. **15**, 1410 (2016).
[12] P. C. Bressloff and S. D. Lawley, J. Phys. A **48** (2015).
[13] P. C. Bressloff and S. D. Lawley, Phys. Rev. E **92** (2015).
[14] C. Doering, in *Stochastic Processes in Physics, Chemistry, and Biology* (Springer, 2000) pp. 316–326.
[15] G. Handy, S. Lawley, and A. Borisyuk, PLoS Comput Biol **14** (2018).

[16] See Supplemental Material for details regarding the estimation of parameters γ and ν, the technical details backing the mathematical assertions made in the main text, two supplemental figures, and one supplemental table, .
[17] P. Guttorp, *Stochastic Modeling of Scientific Data* (Chapman & Hall/CRC, 1995).
[18] P. Metzner, E. Dittmer, T. Jahnke, and C. Schütte, Journal of Computational Physicse **227**, 353 (2007).
[19] H. Bhat, L.-H. Huang, and S. Rodriguez, in *MLSA15, Workshop at ECML/PKDD* (2015).
[20] C. Gardiner, in *Stochastic methods* (Springer, 2010) pp. 264–300.
[21] "Wolfram Research, Inc., Mathematica, Version 11.1," (2017), champaign, IL.
[22] E. Weisstein, From MathWorld–A Wolfram Web Resource.
[23] J. Xia, X. Zhang, J. Staudinger, and R. L. Huganir, Neuron **22**, 179 (1999).
[24] C. Ribrault, K. Sekimoto, and A. Triller, Nature Reviews — Neuroscience **12**, 375 (2011).
[25] L. Ostroff, C. Cain, N. Jindal, N. Dar, and J. Ledoux, Journal of Comparative Neurology **520**, 295 (2012).
[26] G. Nyĺri, F. Stephenson, and P. Freund, T.F. Somogyi, Neuroscience **119**, 347 (2003).
[27] S. Wang, A. Alousi, and S. Thompson, J Gen Physiol. **105**, 149 (1995).